PNAS
www.pnas.org

Supplementary Information for

Predicting the effect of confinement on the COVID-19 spread using machine learning enriched with satellite air pollution observations

Xiaofan Xing[1†], Yuankang Xiong[1†], Ruipu Yang[1†], Rong Wang[1,2,3,4,5,6*], Weibing Wang[7], Haidong Kan[7], Tun Lu[8], Dongsheng Li[9], Junji Cao[10], Josep Peñuelas[11,12], Philippe Ciais[13,14], Nico Bauer[15], Olivier Boucher[16], Yves Balkanski[13], Didier Hauglustaine[13], Guy Brasseur[17,18], Lidia Morawska[19], Ivan A. Janssens[20], Xiangrong Wang[1,4], Jordi Sardans[11,12], Yijing Wang[1], Yifei Deng[1], Lin Wang[1,2,3], Jianmin Chen[1,2,3], Xu Tang[1,2,3], Renhe Zhang[1,2,3]

[1]Shanghai Key Laboratory of Atmospheric Particle Pollution and Prevention, Department of Environmental Science and Engineering, Fudan University, Shanghai 200438, China.
[2]IRDR International Center of Excellence on Risk Interconnectivity and Governance on Weather/Climate Extremes Impact and Public Health (WECEIPHE), Fudan University, Shanghai 200438, China.
[3]Department of Atmospheric and Oceanic Sciences, Institute of Atmospheric Sciences, Fudan University, Shanghai 200438, China.
[4]Center for Urban Eco-Planning & Design, Fudan University, Shanghai 200438, China.
[5]Big Data Institute for Carbon Emission and Environmental Pollution, Fudan University, Shanghai 200438, China.
[6]Shanghai Institute of Pollution Control and Ecological Security, Shanghai 200092, China.
[7]Key Laboratory of Public Health Safety of the Ministry of Education and National Health Commission, Key Laboratory of Health Technology Assessment, School of Public Health, Fudan University, Shanghai 200438, China.
[8]Shanghai Key Laboratory of Data Science, School of Computer Science, Fudan University, Shanghai 200438, China.
[9]Microsoft Research Asia, Shanghai 200232, China.
[10]Institute of Atmospheric Physics, Chinese Academy of Sciences, Beijing 100029, China.
[11]CREAF, Cerdanyola del Vallès, Catalonia 08193, Spain.
[12]CSIC, Global Ecology Unit CREAF-CSIC-UAB, Bellaterra, Catalonia 08193, Spain.
[13]Laboratoire des Sciences du Climat et de l'Environnement, CEA CNRS UVSQ, Gif-sur-Yvette 91190, France.
[14]Climate and Atmosphere Research Center (CARE-C) The Cyprus Institute 20 Konstantinou Kavafi Street, 2121, Nicosia, Cyprus.
[15]Potsdam Institute for Climate Impact Research (PIK), Member of the Leibniz Association, Potsdam 14412, Germany.
[16]Institut Pierre-Simon Laplace, Sorbonne Université /CNRS, Paris 75252, France.
[17]Environmental Modeling Group, Max Planck Institute for Meteorology, Hamburg 20146, Germany.
[18]Atmospheric Chemistry Observations and Modeling Laboratory, National Center for Atmospheric Research, Boulder 80307, USA.
[19]Queensland University of Technology, 2 George Street, Brisbane, QLD 4001, Australia.
[20]Department of Biology, University of Antwerp, Wilrijk B2610, Belgium.
†These authors contributed equally.
* Correspondence to Rong Wang.

This PDF file includes:

Figures S1 to S19
Tables S1 to S2

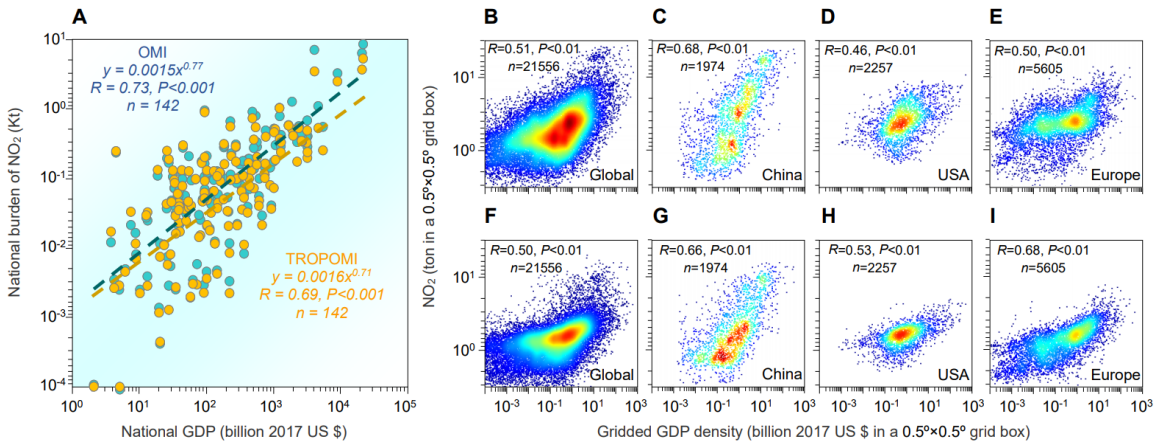

Fig. S1. Relationship between the tropospheric vertical column density of nitrogen dioxide (NO_2) and gross domestic product (GDP). (**A**) Plot of NO_2 burden averaged for 2016–2019 and area of all pixels in a country against the national GDP (purchasing-power-parity) as an average for 2016–2019 across 142 countries with full data of NO_2. NO_2 are retrieved from the backscattered radiance and solar irradiance measured by the Ozone Monitoring Instrument (OMI) on board the US NASA Aura satellite (blue circles) or the Tropospheric Monitoring Instrument (TROPOMI) on board the European Copernicus Sentinel-5 Precursor satellite (orange circles). (**B–I**) As (**a**), but for 0.5º×0.5º grids globally (**B, F**), and in China (**C, G**), the USA (**D, H**) and Europe (**E, I**) using the OMI (**B–E**) or TROPOMI (**F–I**) data.

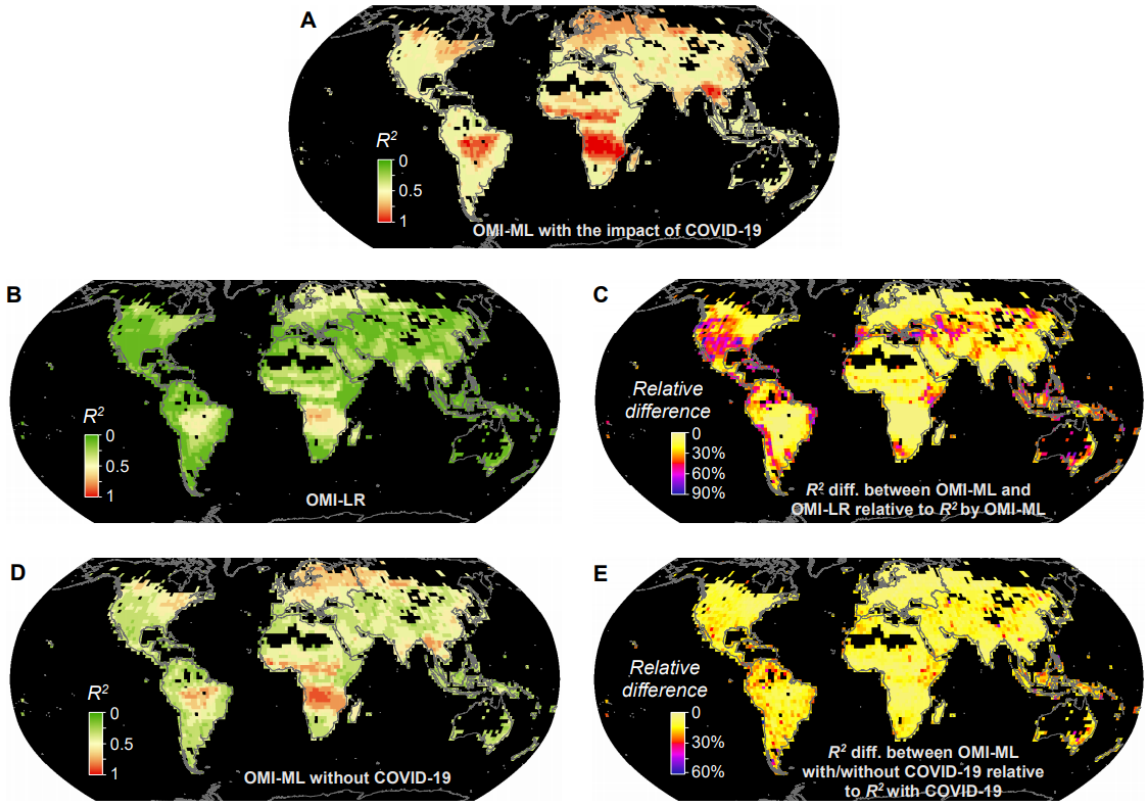

Fig. S2. Variation in tropospheric vertical column density of nitrogen dioxide (NO_2) explained by a fixed-effects model. We fit the fixed-effects model to predict daily NO_2 by accounting for non-linear impacts of meteorology, linear impacts of seasonality and inter-annual trends, and weekly impact of COVID-19 using a dummy variable (see $x_{t,w}$ in **Eq. 1** in **Methods**) on daily NO_2. (**A**) Fraction of day-to-day variations in OMI NO_2 explained by fixed-effects model using machine learning (OMI-ML) as a coefficient of determination (R^2) in global 0.5º×0.5º grids. (**B**) R^2 in a multiple linear regression model (OMI-LR) using the same predictors. (**C**) Difference in R^2 between (**B**) and (**A**) as a percentage relative to (**A**). (**D**) R^2 without considering the impact of COVID-19 by fixing $x_{t,w}$=0 (OMI-ML without COVID-19). (**E**) Difference in R^2 between (**D**) and (**A**) as a percentage relative to (**A**).

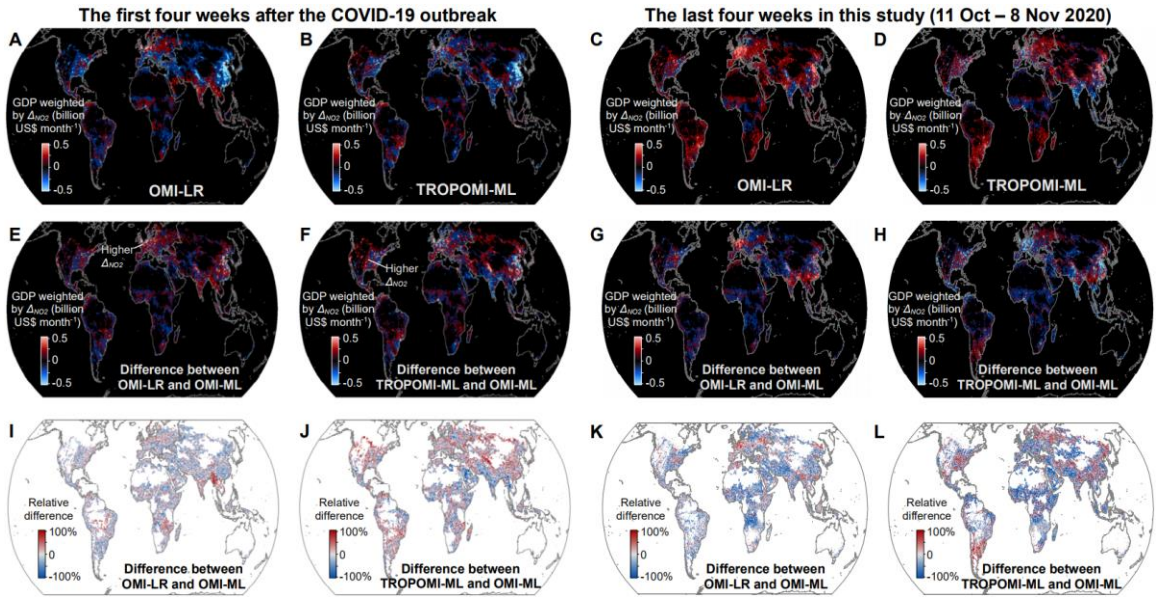

Fig. S3. Changes in tropospheric vertical column density of nitrogen dioxide (NO_2) estimated by a multiple linear model or using the Tropospheric Monitoring Instrument (TROPOMI) data. (**A–D**) Distributions of GDP weighted by Δ_{NO2} in the first four weeks after the COVID-19 outbreak in each region (**A, B**) or the last four weeks for 11 October to 8 November 2020 in this study (**C, D**). In (**A, C**), Δ_{NO2} is estimated using the Ozone Monitoring Instrument (OMI) NO_2 by multiple linear regression (OMI-LR), rather than the machine-learning method (OMI-ML). In (**B, D**), Δ_{NO2} is estimated using the TROPOMI data of NO_2 with machine learning (TROPOMI-ML), rather than the OMI NO_2 (OMI-ML). (**E–L**) Absolute (**E–H**) and relative differences (**I–L**) in GDP weighted by Δ_{NO2} relative to that using the OMI NO_2 data based on a machine-learning method (OMI-ML), as shown in Figs. 1A, B in the main text.

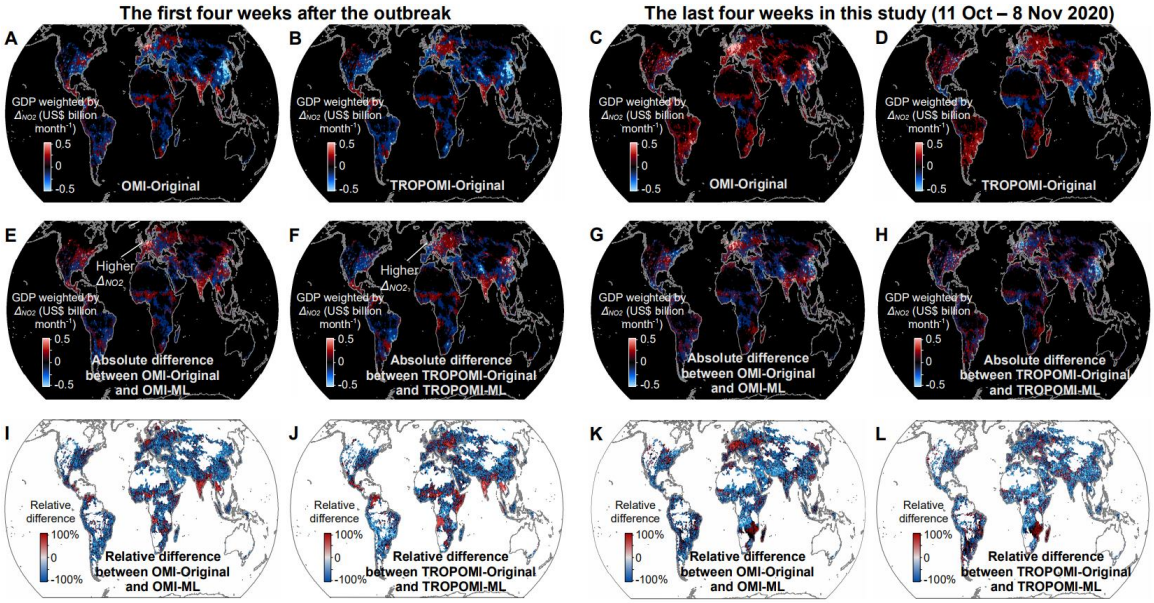

Fig. S4. Changes in tropospheric vertical column density of nitrogen dioxide (NO_2) measured by the Ozone Monitoring Instrument (OMI) and the Tropospheric Monitoring Instrument (TROPOMI) instruments without representing the impact of meteorology. (**A–D**) Distributions of GDP weighted by Δ_{NO2} without considering the impact of meteorology using the (**A, C**) OMI (OMI-Original) or (**B, D**) TROPOMI (TROPOMI-Original) data for NO_2. (**A, B**) for the first four weeks after the COVID-19 outbreak in each region, and (**c, d**) for the last four weeks for 11 October to 8 November 2020 in this study. (**E–L**) Absolute (**E–H**) and relative (**I–L**) differences in GDP weighted by Δ_{NO2} using the OMI data (**E, G, I, K**) relative to results obtained by filtering the impact of meteorology with machine learning (OMI-ML) in Figs. 1a, b, or using the TROPOMI data (**F, H, J, L**) relative to results obtained by filtering the impact of meteorology with machine learning (TROPOMI-ML) in **Figs. S3B, D**.

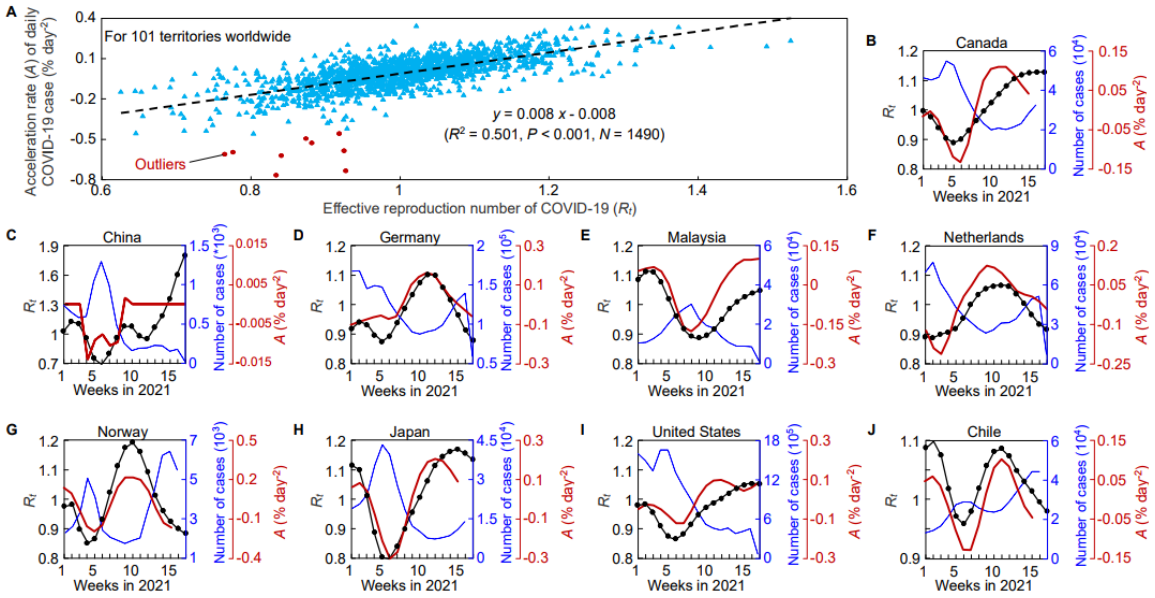

Fig. S5. Comparison between the calculated acceleration of daily COVID-19 cases (*A*) and the reported effective reproduction number (R_t) in the literature (Abbott et al., 2020). (**A**) Scatter plot of *A* and R_t for 101 territories by week in the winter of 2020/21. The squared correlation coefficient (R^2) between *A* and R_t was calculated after excluding 9 outliers (red circles) among 1499 data points by the Grubbs' test at a significance of 0.05. (**B-J**) Time series of A and Rt in Canada (**B**), China (**C**), Germany (**D**), Malaysia (**E**), Netherlands (**F**), Norway (**G**), Japan (**H**), United States (**I**), and Chile (**J**) by week.

Reference:

Abbott, S., Hellewell, J. & Funk, S. Estimating the time-varying reproduction number of SARS-CoV-2 using national and subnational case counts. *Wellcome Open Research*, **5**, 112 (2020).

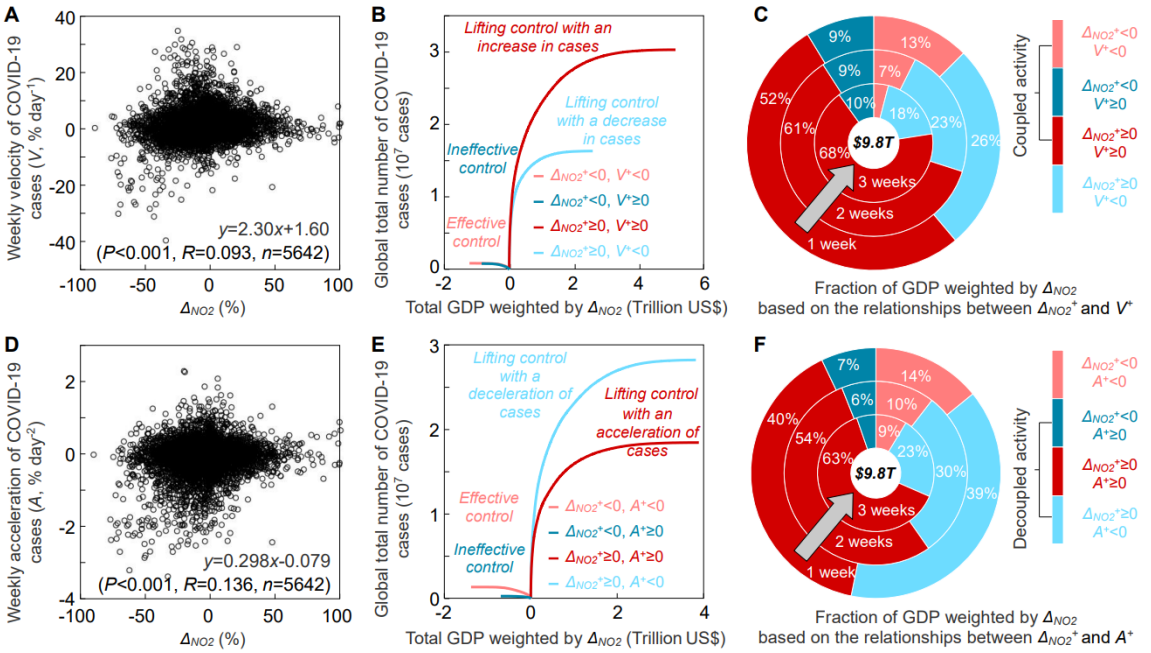

Fig. S6. Relationship between weekly changes in OMI NO_2 (Δ_{NO2}) as an indicator of activity changes during COVID-19 and the weekly velocity (V) or acceleration (A) of daily COVID-19 cases. (**A**) Weekly velocity of COVID-19 cases reported by the European Centre for Disease Prevention and Control (ECDPC) against weekly Δ_{NO2} from 1 Jan. to 8 Nov. 2020 in 211 territories. (**B**) COVID-19 cases as a function of GDP weighted by Δ_{NO2} based on the upper bounds (mean + standard error) of Δ_{NO2} (Δ_{NO2}^+) and velocity (V^+). We divide 5642 pairs of data for cases and GDP weighted by Δ_{NO2} into four regimes: (I) $\Delta_{NO2}^+<0$ and $V^+<0$, (II) $\Delta_{NO2}^+<0$ and $V^+\geq0$, (III) $\Delta_{NO2}^+\geq0$ and $V^+\geq0$ and (IV) $\Delta_{NO2}^+\geq0$ and $V^+<0$. In each regime, we add the number of COVID-19 cases and GDP weighted by Δ_{NO2} one by one, in order of the ratio of cases to the GDP weighted by Δ_{NO2}. The total number of COVID-19 cases is plotted against the total GDP weighted by Δ_{NO2} one in each regime. (**C**) Fraction of GDP weighted by Δ_{NO2} in four regimes. A negative Δ_{NO2}^+ is considered as $\Delta_{NO2}^+<0$ lasting for 1, 2 and 3 consecutive weeks before this week from the outer to the inner pies. Total GDP weighted by Δ_{NO2} is US$9.8 trillion (T) or 8% as an average of Δ_{NO2} weighted GDP. (**D–F**) as (**A–C**), except for weekly acceleration of COVID-19 cases (A) and the upper bound (A^+).

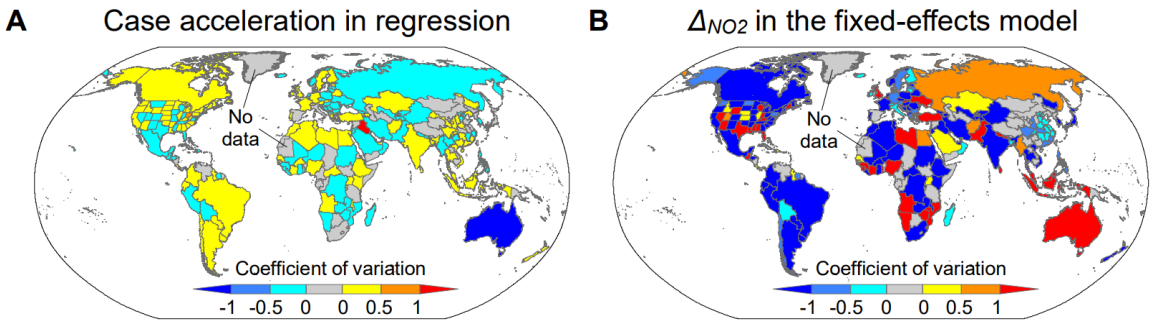

Fig. S7. Coefficient of variation in the case acceleration and Δ_{NO2}. (**a-b**) Coefficient of variation of case acceleration estimated by the regression model (**A**) and Δ_{NO2} estimated by the fixed-effects model (**B**) for each territory. Gray color indicates no data.

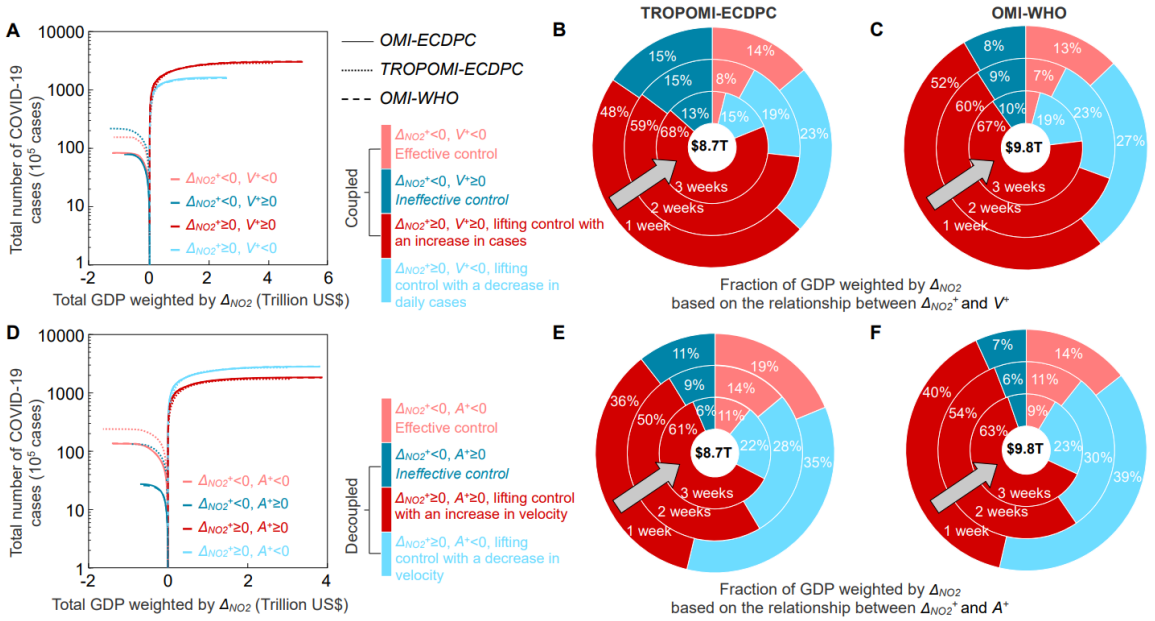

Fig. S8. Relationships between weekly changes in tropospheric vertical column density of nitrogen dioxide (NO_2) (Δ_{NO2}) and the weekly velocity and acceleration of COVID-19 cases using different data. (**A,D**) as **Figs. S5B, E**, but for using NO_2 measured by the Ozone Monitoring Instrument (OMI) or Tropospheric Monitoring Instrument (TROPOMI) instruments and using daily COVID-19 cases reported by the European Centre for Disease Prevention and Control (ECDPC) or the World Health Organization (WHO). (**B, E**) as the **Figs. S5C, F**, but for using NO_2 measured by the TROPOMI (rather than OMI). (**C, F**) as the **Figs. S5C, F**, but for using daily COVID-19 cases reported by the WHO (rather than ECDPC). In (**B, E**), total GDP weighted by Δ_{NO2} is **–**$8.7 trillion (T). In (**C, F**), total GDP weighted by Δ_{NO2} is **–**$9.8 trillion (T).

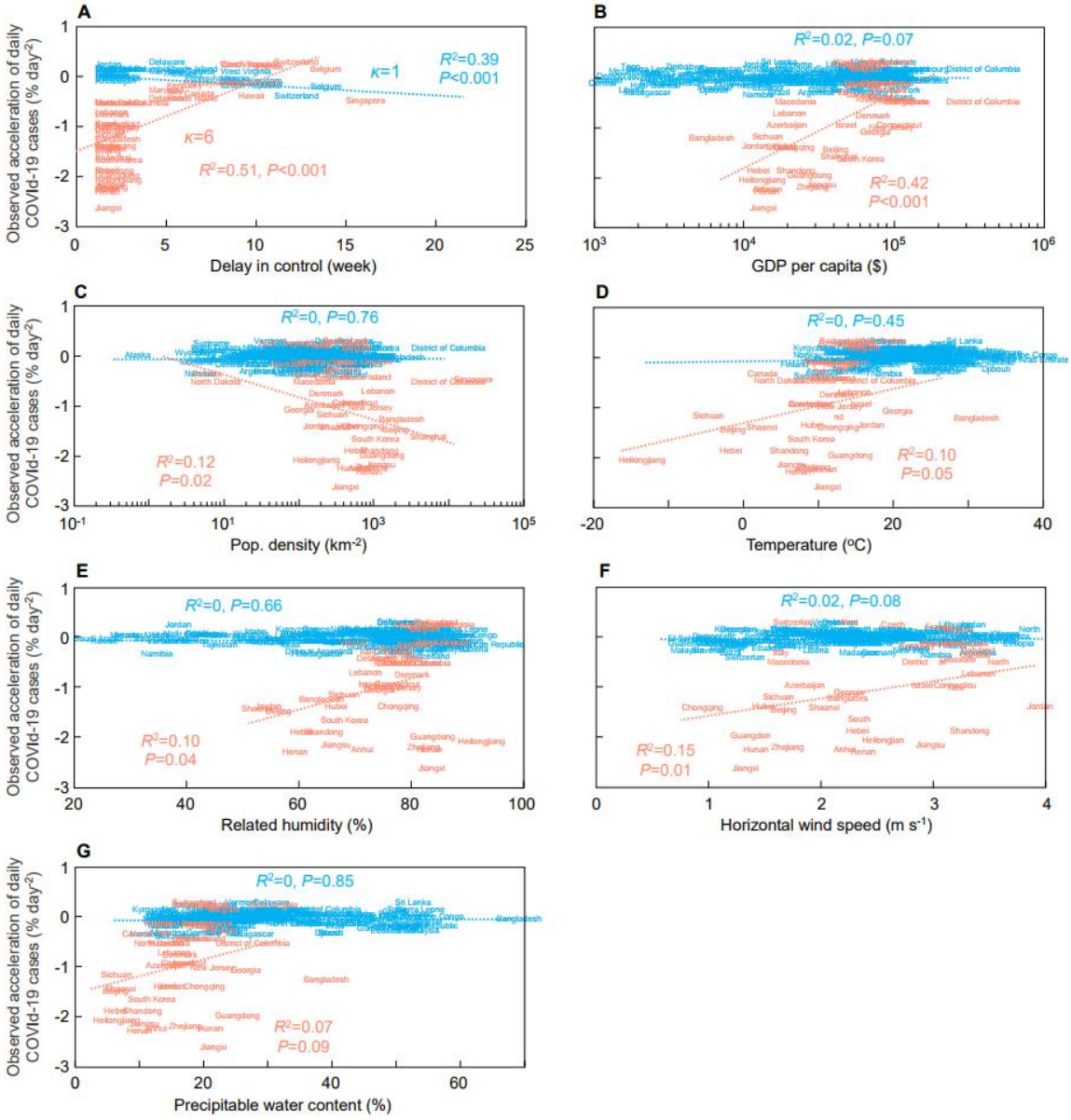

Fig. S9. Relationship between the weekly acceleration of daily COVID-19 cases (*A*) and socioeconomic and environmental indicators. The observed *A* is plotted against the delay in confinement as the number of weeks between the COVID-19 outbreak and the first week with $\Delta_{NO2}^{+}<0$ (**A**), purchasing-power-parity GDP per capita (**B**), average population density (**C**), ambient surface temperature (**D**), relative humidity (**E**), horizontal wind speed (**F**), and precipitable water content in the air (**G**). Each indicator is averaged over weeks in a territory where the upper bound (mean + standard error) of Δ_{NO2} (Δ_{NO2}^{+}) is positive (blue, κ=1) or negative (red, κ=6) for 3 consecutive weeks before these weeks.

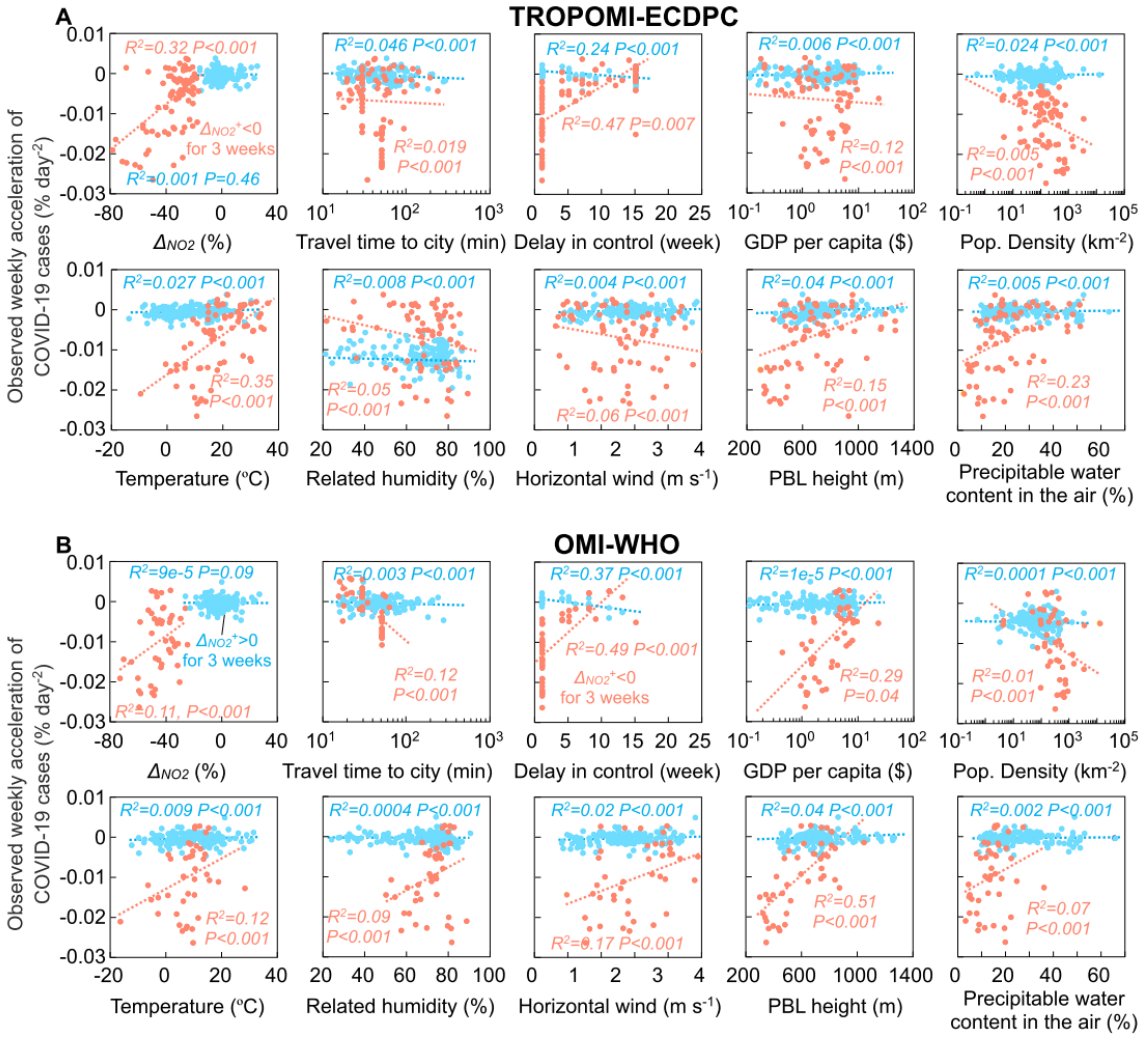

Fig. S10. Effects of socioeconomic and meteorological indicators on acceleration of daily COVID-19 cases (*A*) using different data. (**A**) Plots of the observed weekly acceleration of COVID-19 cases against 10 socioeconomic and environmental indicators, using NO_2 measured by the Tropospheric Monitoring Instrument (TROPOMI) and daily COVID-19 cases reported by the European Centre for Disease Prevention and Control (ECDPC). The indicator is derived as an average in each region for weeks when the upper bound (mean + standard error) of Δ_{NO2} (Δ_{NO2}^{+}) is positive (blue, κ=1) or negative (red, κ=6) for 3 weeks. The correlation coefficient (R) is listed in the panel with P<0.001. PBL, planetary boundary layer. (**B**) as (**A**), except for using NO_2 measured by the Ozone Monitoring Instrument (OMI) and daily COVID-19 cases reported by the World Health Organization (WHO).

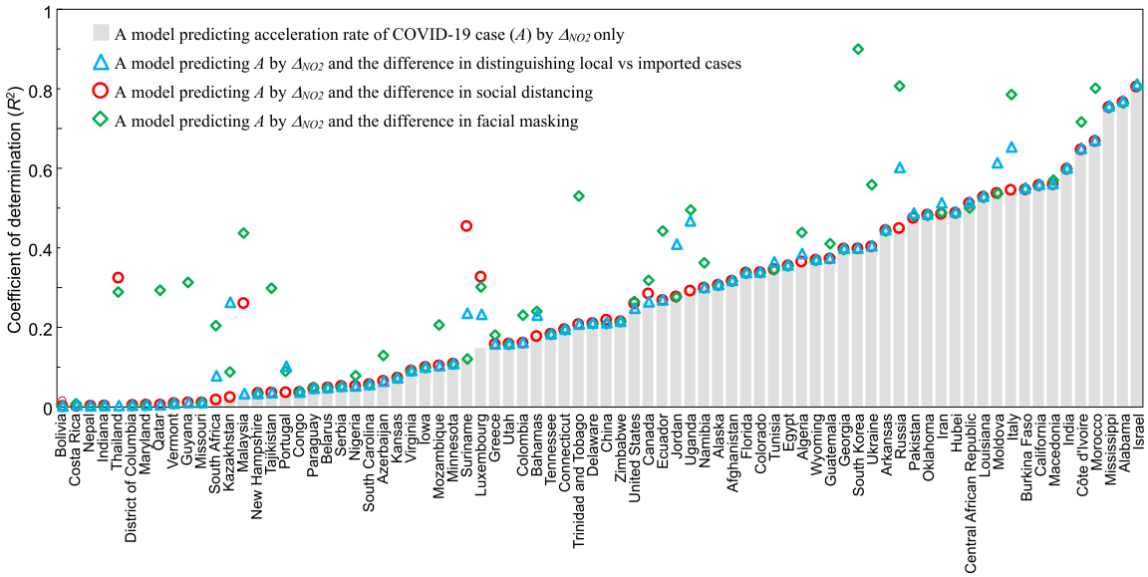

Fig. S11. Coefficient of determination (R^2) in the model predicting the weekly acceleration of daily COVID-19 cases (A) by Δ_{NO2}. The R^2 to predict A by Δ_{NO2} alone (gray column) is compared to that by taking the difference in distinguishing local vs imported cases (triangle), social distancing (circle) or facial masking (diamond) as a covariate.

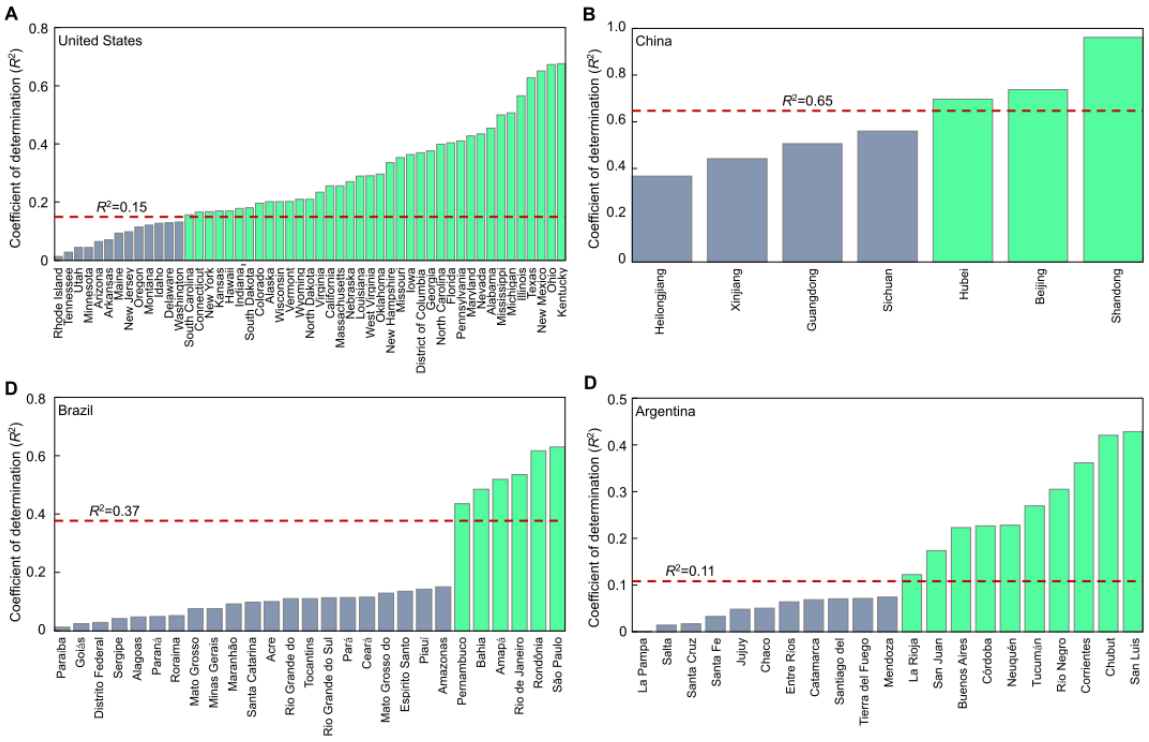

Fig. S12. Coefficient of determination (R^2) in the model to predict the weekly acceleration of daily COVID-19 cases (A) by Δ_{NO2} for provinces or states. (**A**) 51 states in the USA. (**B**) 8 provinces in China (cases information is missing in 23 other provinces). (**C**) 27 states in the Brazil. (**D**) 24 states in the Argentina. The R^2 to predict A by Δ_{NO2} for each state / province (column) is compared to that taking the states / provinces as a whole for each country (dashed line). The green column indicates that R^2 is higher for each state / province than that taking the states / provinces as a whole for each country.

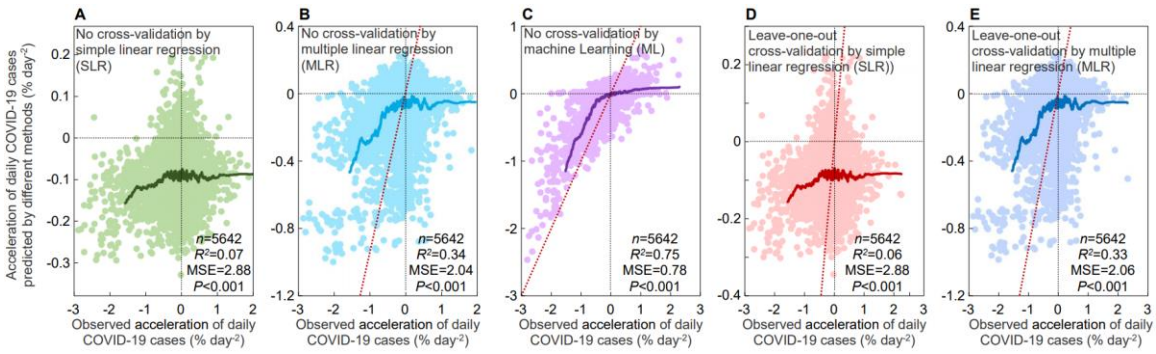

Fig. S13. Comparison of the predicted weekly acceleration of COVID-19 cases to observations with or without cross validation using different methods. Without cross validation, the weekly acceleration of COVID-19 cases (*A*) is predicted (**A**) from NO_2 change (Δ_{NO2}) as a single predictor by simple linear regression, (**B**) Δ_{NO2} and other 10 socioeconomic and environmental indicators as predictors by multiple linear regression, and (**C**) Δ_{NO2} and other 10 socioeconomic and environmental indicators as predictors by machine learning. In leave-one-out cross-validation, *A* is predicted (**D**) from NO_2 change (Δ_{NO2}) as a single predictor using simple linear regression and (**E**) Δ_{NO2} and other 10 socioeconomic and environmental indicators as predictors using multiple linear regression. To better evaluate the prediction of deceleration, the mean squared error (MSE) is weighted by a function of $(0.99)^h$, where *h* is the rank of the observed *A*, while the coefficient of determination (R^2) is defined as one minus the ratio of MSE to variance in the observed *A*. The moving averages are shown at an interval of 50 (thick lines).

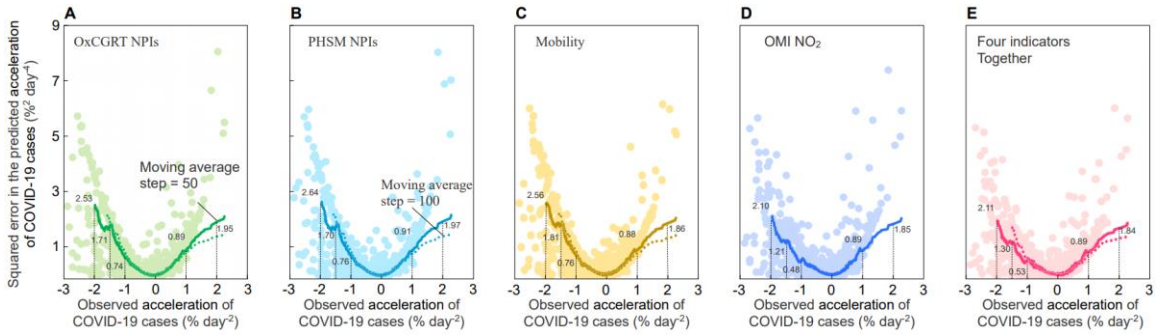

Fig. S14. Residual analysis for the five machine-learning models using different predictors in leave-one-out cross-validation. Squared errors of the predicted weekly acceleration of daily COVID-19 cases using the OxCGRT NPIs (**A**), the PHSM NPIs (**B**), the Google/Baidu human mobility (**C**) or OMI NO_2 change (Δ_{NO2}) (**D**) as the predictor. In these machine-learning models, socioeconomic and environmental indicators used as other predictors are identical. In (**A–D**), the moving averages of the squared errors are shown at an interval of 50 (solid line) or 100 (dashed line). (**E**) as (**A–D**), but for using the OxCGRT NPIs, the PHSM NPIs, human mobility and Δ_{NO2} together with 10 socioeconomic and environmental indicators as the predictors.

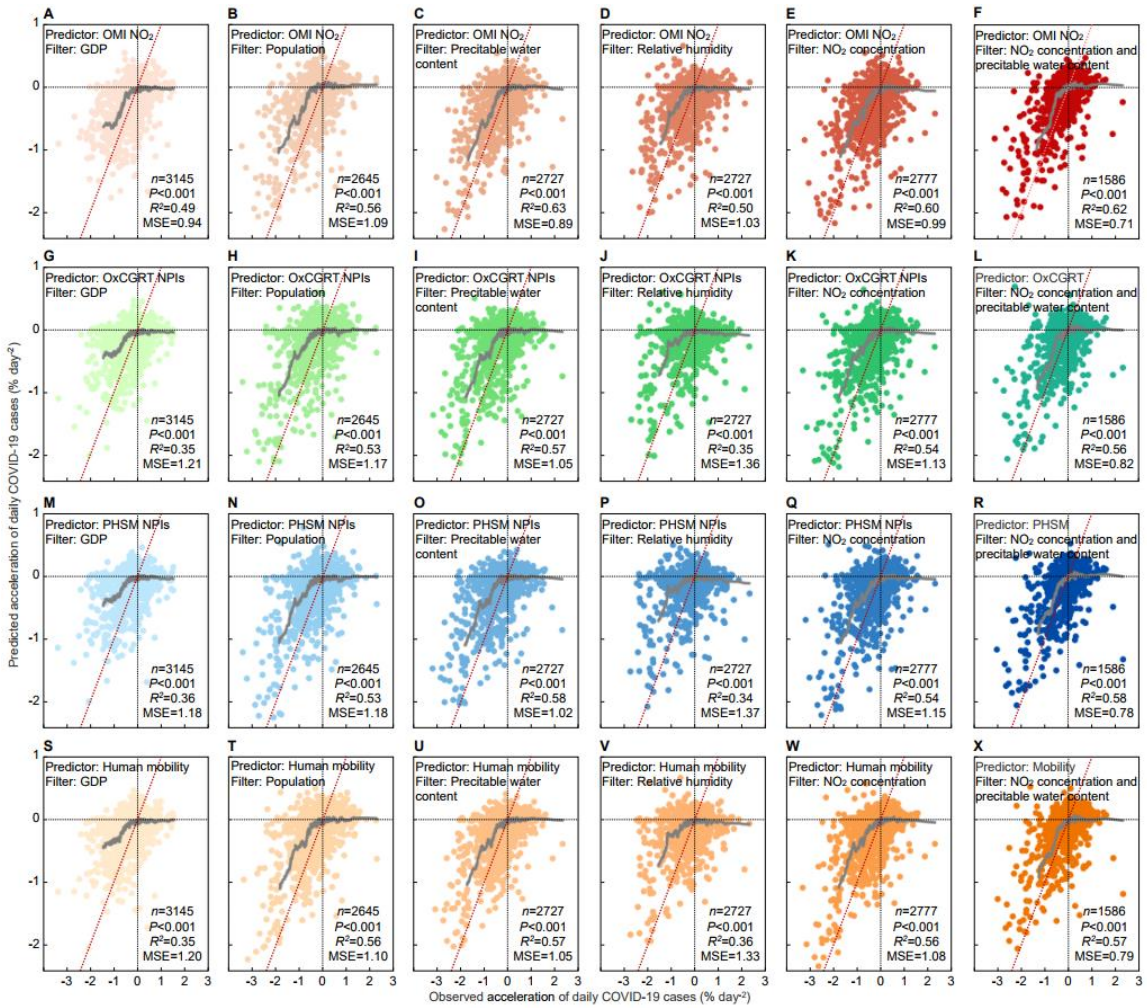

Fig. S15. Comparison of the predicted weekly acceleration of daily COVID-19 cases (*A*) to observations in leave-one-out cross-validation by filtering data with different thresholds. *A* is predicted using NO_2 change (Δ_{NO2}) (**A–F**) or alternatively using the OxCGRT NPIs (**G–L**), the PHSM NPIs (**M–R**) and the Google/Baidu human mobility (**S–X**) as a predictor, while 10 socioeconomic and environmental indicators as other predictors are identical. We filter data with precitable water content in the air and relative humidity above the median, or GDP, population and NO_2 column concentration below the median. Because R^2 of *A* increases remarkably by filtering data with precitable water content in the air and NO_2 column concentration, we show the performance by filtering data with these two indicators together in (**F, L, R, X**). The moving averages are shown at an interval of 50 (thick lines).

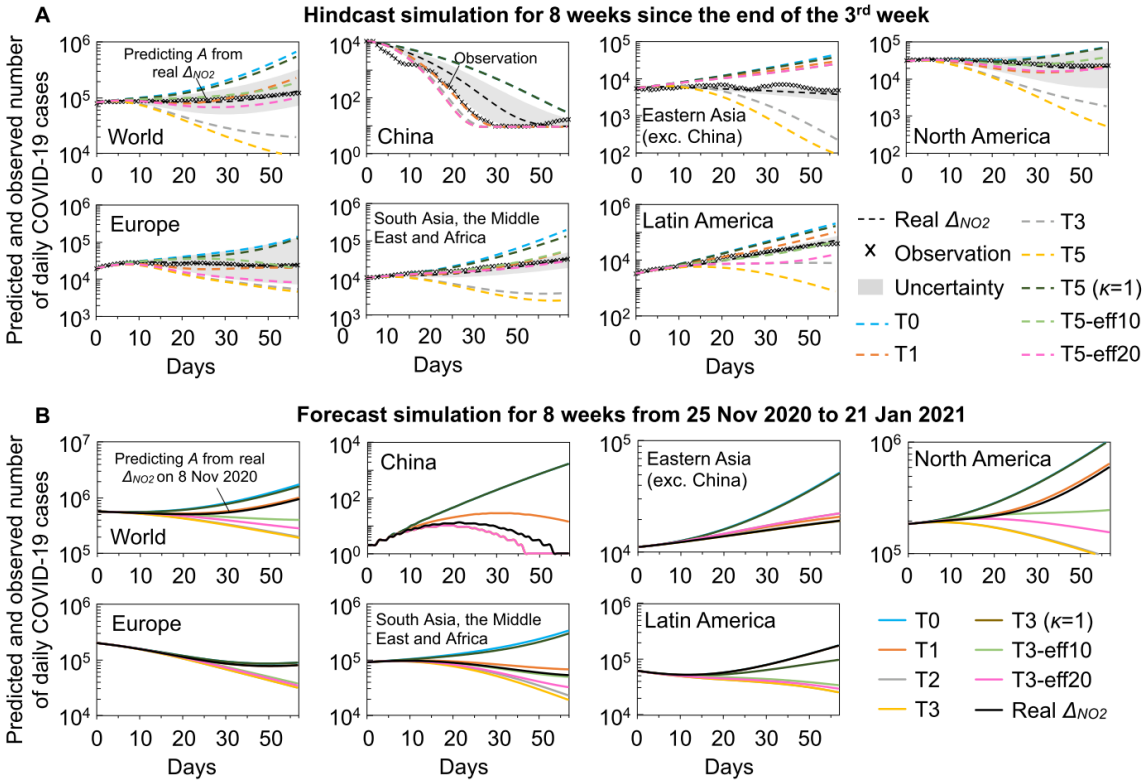

Fig. S16. Hindcast and forecast simulations of daily COVID-19 cases. Hindcast (**A**) and forecast (**B**) simulations of new COVID-19 cases over 8 weeks since the end of the 3rd week after the COVID-19 outbreak or since 25 Nov. 2020. In hindcast simulation scenario, we considered 8 scenarios using the real Δ_{NO2}, constant Δ_{NO2} of 0 (T0), –10% (T1), –30% (T3) and –50% (T5) in all territories, T5 with the discrete variable κ held at 1, and Δ_{NO2} of –50% in the 10% (T5-eff10) and 20% (T5-eff20) of territories with the highest sensitivity of A to Δ_{NO2}. In forecast simulation scenario, we considered 8 scenarios as those in hindcast simulation scenario, but for Δ_{NO2} of 0 (T0), –10% (T1), –20% (T2) and –30% (T3).

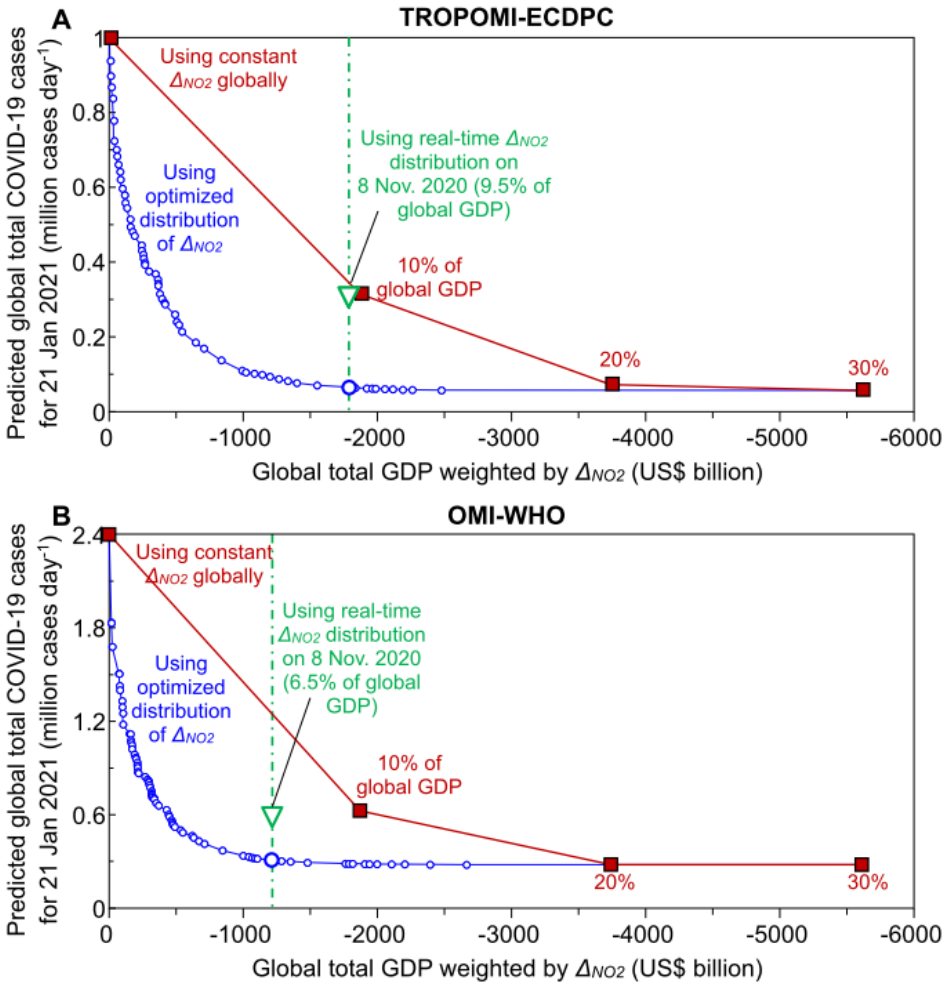

Fig. S17. Dependences of daily COVID-19 cases for 21 January 2021 on the global total GDP weighted by Δ_{NO2} using different data inputs. (**A**) as Fig. 6A, except for using tropospheric vertical column density of nitrogen dioxide (NO_2) measured by the Tropospheric Monitoring Instrument (TROPOMI) and daily COVID-19 cases reported by the European Centre for Disease Prevention and Control (ECDPC). (**B**) as Fig. 6A, except for using NO_2 measured by the Ozone Monitoring Instrument (OMI) and daily COVID-19 cases reported by the World Health Organization (WHO).

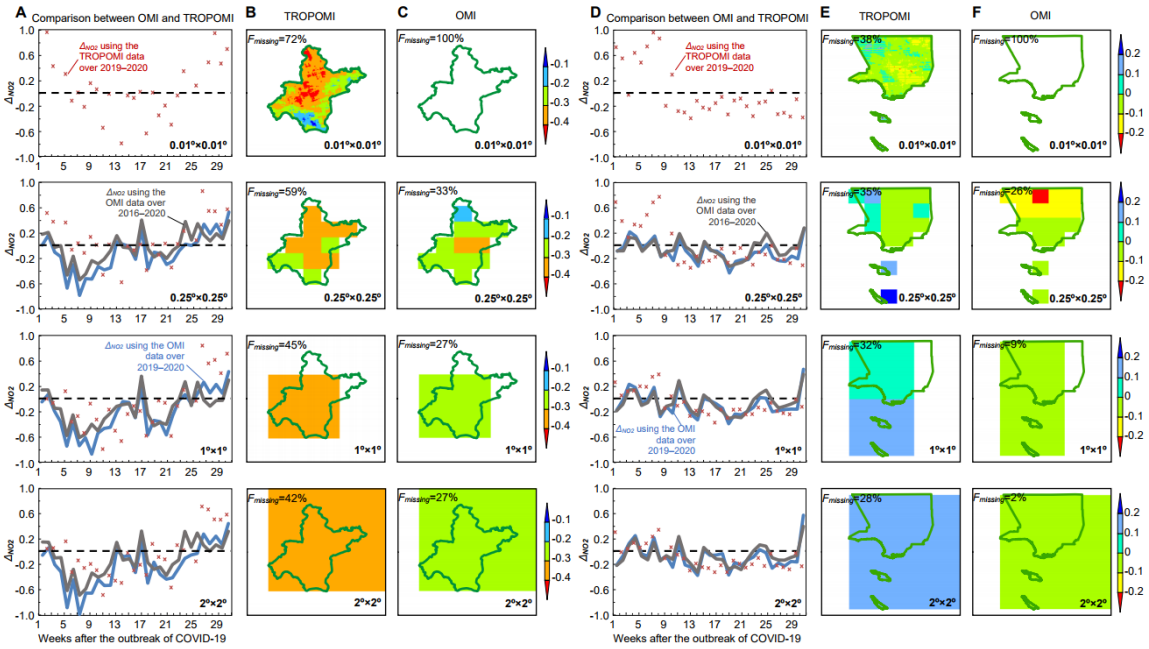

Fig. S18. Comparison of tropospheric vertical column density of nitrogen dioxide (NO_2) measured by the Ozone Monitoring Instrument (OMI) and the Tropospheric Monitoring Instrument (TROPOMI). The OMI and TROPOMI data are used to estimate NO_2 change (Δ_{NO2}) in Wuhan, China (**A–C**) and Los Angeles, the USA (**D–F**). (**A, D**) Comparison of Δ_{NO2} using the OMI (2016–2020) and TROPOMI (2019–2020) data at a resolution of 0.01º×0.01º, 0.25º×0.25º, 1º×1º and 2º×2º, respectively. To show the influence of a longer period measuring data by the OMI (2016–2020) than the TROPOMI (2019–2020) instrument, the estimated Δ_{NO2} using the OMI data for 2016–2020 (grey line) is compared to that using the OMI data only for 2019–2020 (blue line). (**B, E**) Distribution of Δ_{NO2} using TROPOMI data for 2019–2020. (**C, F**) Distribution of Δ_{NO2} using OMI data for 2016–2020. The fraction of missing data ($F_{missing}$) is given in (**B, C, E, F**).

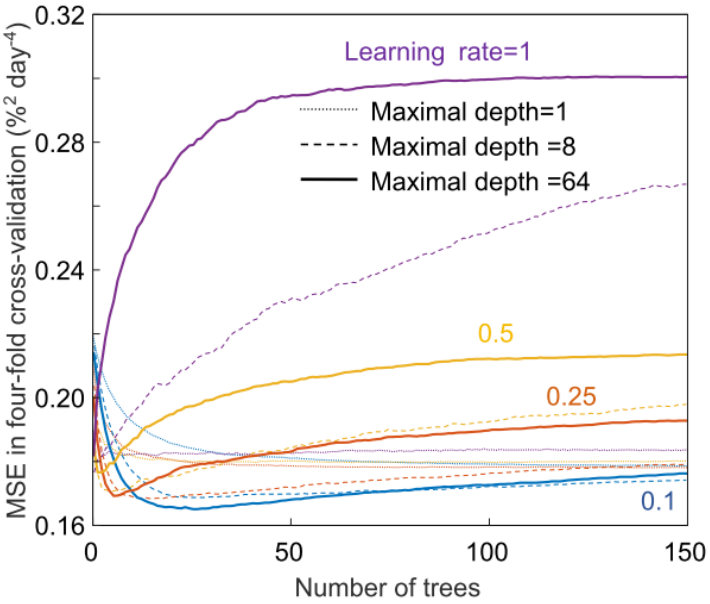

Fig. S19. Optimization of the model predicting the weekly acceleration of daily COVID-19 cases (*A*) from NO_2 change (Δ_{NO2}) along with 10 socioeconomic and environmental indicators by machine learning. To evaluate the model performance under different parameters adopted for machine learning, we plot the dependence of the mean square error (MSE) in the four-fold cross-validation on the maximum depth of each tree, learning rate and the number of trees in the gradient-boosting-decision-tree regression.

Table S1. Time of lockdowns in typical regions or countries.

Region	1st lockdown		2nd lockdown		Data sources
	Start	End	Start	End	
France	3.17	5.11	10.30	12.01	Flaxman, S. et al. Estimating the effects of non-pharmaceutical interventions on COVID-19 in Europe. *Nature* **584**, 257-261 (2020).
Italy	3.09	5.18	11.06	12.03	
Spain	3.14	5.09	-	-	
UK	3.23	7.04	11.05	12.02	
Germany	3.23	5.10	11.02	11.30	
Singapore	4.07	6.01	-	-	
Korea	-	-	-	-	https://en.wikipedia.org/wiki/COVID-19_pandemic_lockdowns
Japan	-	-	-	-	
Beijing	2.10	4.30	-	-	http://www.gov.cn/xinwen
Wuhan	1.23	4.08	-	-	http://www.gov.cn/xinwen
Shanghai	2.10	3.24	-	-	http://wap.sh.gov.cn/nw2/nw2314/nw2319/nw44142/u26aw64656.html
India	3.25	6.07	-	-	
Iran	3.14	4.20	-	-	
Iraq	3.22	4.11	-	-	
South Africa	3.26	4.30	-	-	
Turkey	4.23	4.27	-	-	
Peru	3.16	6.30	-	-	
Argentina	3.29	5.04	-	-	https://en.wikipedia.org/wiki/COVID-19_pandemic_lockdowns
California	3.19	5.18	-	-	
New York	3.22	6.13	-	-	
Washington	3.25	4.10	-	-	
North Korea	7.25	8.14	-	-	
Vietnam	4.01	4.22	-	-	
Thailand	3.25	5.31	-	-	
São Paulo	3.24	5.10	-	-	

Table S2. Coefficient of determination (R^2) in the prediction of weekly acceleration of COVID-19 cases (A) in leave-one-out cross-validation by filtering data with different thresholds. A is predicted using OMI NO_2 changes (Δ_{NO2}) (**a–f**), or alternatively the OxCGRT NPIs, the PHSM NPIs and human mobility as the predictor, while other predictors are identical. To consider the impact of noises in satellite data, we filter data with precitable water content in the air and relative humidity (related to clouds) above a threshold, or the GDP, population and average NO_2 column concentration below a threshold. Because R^2 of A predicted from Δ_{NO2} increases remarkably by filtering data with precitable water content and average NO_2 column concentration, we show the performance by filtering data with these two indicators together. We select the median or the 75% (p^{75}) and 90% (p^{90}) percentiles as the threshold to filter data.

Filtering variable(s)	Threshold	R^2			
		OMI NO_2	OxCGRT NPIs	PHSM NPIs	Human mobility
GDP	p^{90}	0.55	0.43	0.44	0.42
Population	p^{90}	0.57	0.46	0.43	0.46
Precitable water content	p^{90}	0.56	0.44	0.46	0.45
Relative humidity	p^{90}	0.48	0.36	0.34	0.36
NO_2 concentration	p^{90}	0.55	0.45	0.44	0.44
Precitable water content and NO_2 concentration	**p^{90}**	**0.57**	**0.46**	**0.47**	**0.48**
GDP	p^{75}	0.59	0.45	0.46	0.47
Population	p^{75}	0.55	0.47	0.47	0.45
Precitable water content	p^{75}	0.58	0.46	0.47	0.48
Relative humidity	p^{75}	0.47	0.30	0.30	0.31
NO_2 concentration	p^{75}	0.56	0.43	0.43	0.44
Precitable water content and NO_2 concentration	**p^{75}**	**0.60**	**0.50**	**0.51**	**0.49**
GDP	median	0.49	0.35	0.36	0.35
Population	median	0.56	0.53	0.53	0.56
Precitable water content	median	0.63	0.57	0.58	0.57
Relative humidity	median	0.50	0.35	0.34	0.36
NO_2 concentration	median	0.60	0.54	0.54	0.56
Precitable water content and NO_2 concentration	**median**	**0.62**	**0.56**	**0.58**	**0.57**